Mesoporous $LiFePO_4$/C Nanocomposite Cathode Materials for High Power Lithium Ion Batteries with Superior Performance

By *Guoxiu Wang,* Hao Liu, Jian Liu, Shizhang Qiao,* Gaoqing Max Lu, Paul Munroe,* and *Hyojun Ahn*

Today, we are facing a severe challenge–global warming and climate change due to the burning of fossil fuels for energy. The greenhouse gas emissions are mainly derived from the transportation sector and electricity power generation. Therefore, a global solution must involve a dramatic move to renewable energy.[1,2] Lithium ion batteries have proved themselves the most advanced electrochemical energy storage and conversion system for a wide range of green applications, including hybrid electric vehicles (HEVs), plug-in hybrid electric vehicles (PHEVs), and stationary energy storage for solar and wind electricity generation as well as smart grids. However, the current generation of lithium ion batteries using $LiCoO_2$ as cathode material cannot meet the stringent requirements for high power application in terms of cost, safety and environmental concerns.[3,4] Since its discovery in 1997,[5,6] $LiFePO_4$ has been emerging as a new cathode material for lithium ion batteries, in particular for high power application, owing to its low cost, environmental friendliness, and high thermal stability. $LiFePO_4$ has an orthorhombic olivine crystal structure, (S. G.: Pnma), in which the strong P-O covalency stabilizes the Fe^{3+}/Fe^{2+} redox couple through the Fe-O-X inductive effect, inducing extremely high thermal stability compared to all other cathode candidates for operating at elevated temperature. In addition, $LiFePO_4$ posses a flat discharge potential at 3.4 V vs. Li/Li^+, which is compatible with most existing organic electrolytes. However, $LiFePO_4$ is insulating in nature with a low electric conductivity of around 10^{-11} Scm^{-1} (compared with 10^{-3} Scm^{-1} for $LiCoO_2$ and 10^{-5} Scm^{-1} for $LiMn_2O_4$), inducing low rate capacity. Many efforts have been made to improve the electrochemical performance of $LiFePO_4$, including addition of conductive Cu/Ag nanopowders or carbon black powders,[7–9] doping with supervalent cations,[10,11] coating with carbon layer or metal oxides,[12,13] and preparation of nanocrystalline particles.[14,15]

Recently, the electrochemical performance of $LiFePO_4$ cathode materials has been further improved through nanoengineering.[16,17] Spherical $LiFePO_4$-polyacene nanoparticles were prepared and exhibited a 1 C rate capacity of 130 mAh/g and a 5 C rate capacity around 95 mAh/g.[18] Nanowire and hollow $LiFePO_4$ cathodes were synthesised and achieved good capacity retention at the 15 C rate.[19] In particular, high rate capacity $LiFePO_4$ has been achieved through creating an ion conducting lithium phosphate coating on the surface of $LiFePO_4$ nanoparticles.[20] However, the long term cycling data is not clear. It is a compulsory requirement for lithium ion batteries to have long cycle life for HEV application. Herein, we report on a new strategy to prepare high rate $LiFePO_4$ cathode material with a mesoporous structure, in which electrolyte can easily infiltrate into the mesopores to contact the embedded $LiFePO_4$ nanocrystals. Based on half-cell testing, $LiFePO_4$/C mesoporous nanocomposites achieved a high capacity of 166 mAh/g (approaching its theoretical capacity of 170 mAh/g) at the 0.1 C rate and an ultrahigh rate capacity of 118 mAh/g at the 10 C rate with an excellent cycle life. This result clearly demonstrates that mesoporous $LiFePO_4$/C nanocomposites are high performance cathode materials suitable for high power applications.

Mesoporous $LiFePO_4$/C nanocomposite was prepared by a nanocasting technique. In the first step, mesoporous carbons (CMK-3) were synthesised following a reported method and used as templates.[21] CMK-3 carbons are assemblies of hexagonally ordered carbon rods separated by mesosize pore channels, in which the individual carbon rods are interconnected by carbon spacers.[21] CMK-3 carbons are hydrophobic in nature. Therefore, we treated the templates by concentrated nitric acid to introduce —OH and —COOH functional groups onto the mesoporous carbon surface, inducing hydrophilicity for facile impregnation in the aqueous solution.[22] After that, the modified CMK-3 templates were impregnated with the precursor Li^+, Fe^{2+} and PO_4^{3+} salt solutions. The final products were obtained by sintering at 700 °C in inert atmosphere (see the experimental section). **Figure 1(a)** shows the wide angle X-ray diffraction (XRD) pattern of mesoporous $LiFePO_4$/C nanocomposite, in

[*] Prof. G. X. Wang
Department of Chemistry and Forensic Science
University of Technology
Sydney, Sydney, NSW 2007 (Australia)
E-mail: Guoxiu.Wang@uts.edu.au
Mr. H. Liu, Dr. J. Liu, Assoc. Prof. S. Z. Qiao, Prof. G. M. Lu
ARC Centre of Excellence for Functional Nanomaterials
The University of Queensland
St. Lucia 4072, QLD (Australia)
Email: s.qiao@uq.edu.au
Prof. P. Munroe
Electron Microscope Unit
The University of New South Wales
Sydney, NSW 2052 (Australia)
Prof. H. J. Ahn
School of Materials Science and Engineering
Gyeongsang National University
900 Gazwa-dong, Jinju, Gyeongnam, 660-701 (Korea)

DOI: 10.1002/adma.201002045

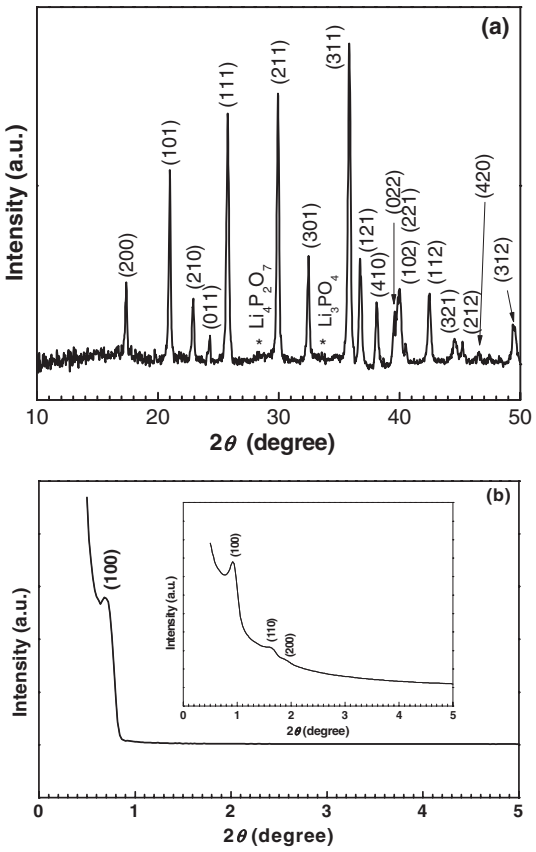

Figure 1. (a) Powder X-ray diffraction pattern of mesoporous $LiFePO_4$/C nanocomposite. (b) Small angle X-ray diffraction pattern of $LiFePO_4$/C nanocomposite. The inset is the SAXRD pattern of the original CMK-3 carbon template.

which the majority of diffraction lines can be indexed to the orthorhombic $LiFePO_4$ phase. We note that very small amounts of impurity phases are also present, which can be identified as $Li_4P_2O_7$ and Li_3PO_4, respectively. These minor impurities could have been induced during the sintering process due to the highly reducing environment and, they usually exist in the form of nanosized clusters.[23] As previously reported, those impurity phases could have benefits for fast charging and discharging by providing a guest ion-conductive surface.[20,24,25] No crystalline graphite phase can be identified from the XRD pattern, indicating that the mesoporous carbon matrices are amorphous. This has been further confirmed by a Raman spectroscopy measurement as evidenced by the appearance of a strong D peak and weak G peak in the Raman spectrum of the mesoporous $LiFePO_4$/C nanocomposite (Supporting Information (SI) Figure S1). Small angle X-ray diffraction (SAXRD) measurements were performed on both the CMK-3 carbon template and $LiFePO_4$/C nanocomposite (as shown in Figure 1(b)). For the CMK-3 mesoporous carbon template (the inset in Figure 1(b)), the SAXRD peaks can be indexed to the (100), (110), and (200) diffraction lines of the hexagonal mesoporous structure (p6mm), which should be ascribed to the long range regularity and highly ordered nature of the mesoporous structures.[26] After impregnation with $LiFePO_4$ nanoparticles, the (110) and (200) diffraction peaks almost disappear, proving the pore filling effect in the impregnation process. It should be noted that the (100) diffraction line was shifted to the lower angle of 0.7° (compared to 0.92° for the original CMK-3 template), indicating enlargement of the mesopores because of the acid-treatment of CMK-3 carbon templates (see the experimental section).

Nitrogen isothermal adsorption-desorption measurements were performed to determine the pore structure and the Brunauer-Emmett-Teller (BET) surface areas of both the CMK-3 template and the mesoporous $LiFePO_4$/C nanocomposites. The results are presented in Figure S2 (SI), showing typical IV isotherms of a mesoporous structure. The BET surface areas are 1458 m^2/g for CMK-3 template and 190 m^2/g for mesoporous $LiFePO_4$/C nanocomposite. The significant decrease in the BET surface area also confirmed the filling of mesopores in the nanocomposite. The pore size distributions are shown as the insets in Figure S2(a) and (b) respectively. The CMK-3 carbon template has a primary pore size of 6.73 nm, while $LiFePO_4$/C nanocomposite has a pore size distribution with a maximum at about 4.3 nm. The existence of smaller mesopores in the nanocomposite indicates that the large mesopores in the CMK-3 templates were partially filled with $LiFePO_4$ nanoparticles.

The morphology and microstructure of the as-prepared CMK-3 mesoporous carbon templates and the mesoporous $LiFePO_4$/C nanocomposite were analysed by field emission scanning electron microscope (FESEM), transmission electron microscope (TEM) and high resolution (HRTEM) analysis. FESEM images are shown in Figure S3 (SI). CMK-3 carbon templates depict a worm-like morphology and porous structure. After impregnation, $LiFePO_4$/C nanocomposite maintained the same shape and morphology as that of the template, except for that the mesopores were blocked by $LiFePO_4$ nanoparticles. **Figure 2(a)** shows a HRTEM image of a CMK-3 template, in which mesopore channel structures are clearly visible. Selected area electron diffraction (SAED) was performed and is shown as the inset in Figure 2(a). The diffuse SAED rings confirmed the amorphous nature of CMK-3 carbon template. Figure 2(b) shows a TEM view of CMK-3 template along the [001] direction, explicitly illustrating the hexagonal pattern of the P6mm mesoporous structure. In order to investigate the dispersion of $LiFePO_4$ nanoparticles in the CMK-3 mesoporous carbon matrix, we performed TEM and HRTEM observation on the mesoporous $LiFePO_4$/C nanocomposite. Figure 2(c) presents a HRTEM image of a $LiFePO_4$/C nanocomposite bundle, from which it is clearly visible that $LiFePO_4$ particles are embedded in mesopore channels in carbon matrix. Elemental mapping by energy-dispersive X-ray (EDX) spectroscopy confirmed the existence of Fe, P and O (see SI, Figure S4). Figure 2(d) illustrates a HRTEM image of another $LiFePO_4$/C nanocomposite bundles, in which $LiFePO_4$ nanoparticles distributed both inside and outside mesopore channels. $LiFePO_4$ nanoparticles have a size in the range of a few nm to a few tens of nm. Therefore, based on FESEM and TEM observation, we can conclude that $LiFePO_4$/C nanocomposites have a honeycomb microstructure, in which $LiFePO_4$ nanoparticles are distributed in mesoporous carbon framework. Even after filling with $LiFePO_4$ nanoparticles, mesopore channels still exist in the nanocomposite structure, which ensures facile infiltration of electrolyte into the mesopores in lithium ion cells. The weight percentage of $LiFePO_4$

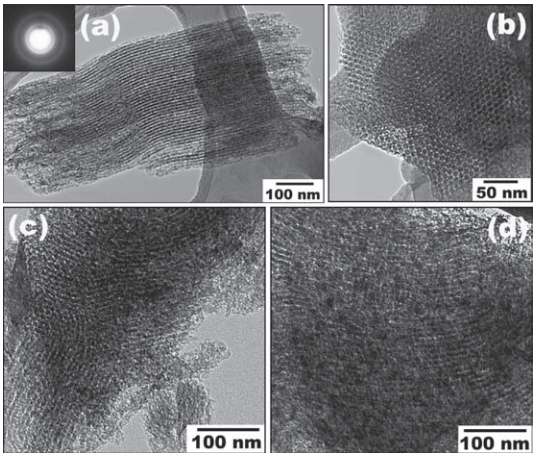

Figure 2. (a) TEM image of a CMK-3 carbon template, showing mesopore channel structure. The inset is the corresponding SAED pattern. (b) TEM view of the CMK-3 carbon template along the [001] direction, illustrating the regular pattern of carbon particles in the mesoporous structure. (c) and (d) HRTEM images of mesoporous $LiFePO_4$/C nanocomposite, showing that $LiFePO_4$ nanoparticles are embedded inside and outside the mesopores.

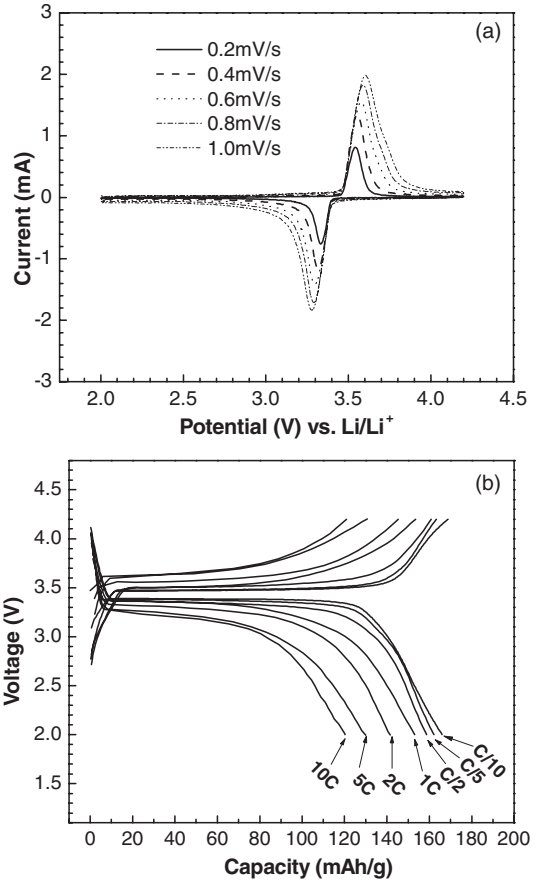

Figure 3. (a) Cyclic voltammograms of mesoporous $LiFePO_4$/C nanocomposite electrode at different scanning rates. (b) The first discharge and charge profiles of $LiFePO_4$/C nanocomposite electrodes at different current rates.

in mesoporous nanocomposite was determined to be 87 wt% by thermogravimetric analysis (TGA, see SI Figure S5).

The electrochemical performance of as-prepared mesoporous $LiFePO_4$/C nanocomposites was evaluated by cyclic voltammetry (CV) and galvanostatic charge/discharge cycling using CR 2032 coin cells. **Figure 3(a)** shows CV curves of $LiFePO_4$/C nanocomposite electrode at different scanning rates. The well defined sharp redox peaks in the range of 3.26 V–3.70 V should be attributed to the Fe^{2+}/Fe^{3+} redox couple reaction, corresponding to lithium extraction and insertion in $LiFePO_4$ crystal structure. Even at the high scanning rate of 1.0 mV/s, the sharp redox reaction peaks are still maintained. Figure 3(b) shows the charge/discharge profiles of mesoporous $LiFePO_4$/C cathodes at different current rates in the first cycle. The nanocomposite electrode delivered a discharge capacity of 166 mAh/g at the 0.1 C rate (10 hours charge and 10 hours discharge), which is very close to the theoretical capacity of $LiFePO_4$ (170 mAh/g). Although the specific capacity gradually decreases with increasing current rate, a high initial capacity of 156 mAh/g capacity has been achieved at the 1 C rate. Even at the high current rate of 10 C, a capacity of 118 mAh/g is still obtained, demonstrating that the as-prepared mesoporous $LiFePO_4$/C nanocomposite can endure high rate charge and discharge. The rate performance of our mesoporous $LiFePO_4$/C nanocomposites is comparable or even better than those of previously reported $LiFePO_4$ composites,[13,18] porous monolithic $LiFePO_4$/C composite,[27] $LiFePO_4$ nanoparticles embedded in nanoporous carbon matrix,[28] and carbon-rich $LiFePO_4$ nanoparticles.[29]

In order to examine the cycle life of mesoporous $LiFePO_4$/C nanocomposite, we performed long-term charge/discharge cycling at different current rates. **Figure 4(a)** shows the cyclability of mesoporous $LiFePO_4$/C cathode at the low current rate of 0.1 C, on which the charge and discharge capacity curves are almost overlapping due to the ultrahigh coulombic efficiency with an average efficiency of almost 100% (as shown in the inset). After 100 cycle, the test cell still delivered a capacity of 162 mAh/g (average 99.96% capacity retention), demonstrating ultra-high cyclability at low current rate for the mesoporous $LiFePO_4$/C nanocomposites (see the capacity retention curve shown in SI Figure S6). We also tested at varied current rates: 0.1 C, 0.2 C, 0.5 C, 1 C, 2 C, 5 C, and 10 C. The results are shown in Figure 4(b). It should be noticed that as long as the current rate reverses back low current rate, the cell capacity can recover to the original value, indicating that the integrity of the mesoporous cathode material has been maintained even after high rate charge and discharge. This clearly demonstrates that our mesoporous material architecture is tolerant to varied charge and discharge current, which is a desirable characteristic required for high power application.

For HEV or PHEV applications, batteries are required to operate at high current density and to have a cycle life of more than 5000 cycles.[30] Therefore, we cycled mesoporous $LiFePO_4$/C nanocomposite electrode at 10 C rate (6 minutes for charging and 6 minutes for discharging) for 1000 cycles (as shown in Figure 4(c)). Surprisingly, our mesoporous $LiFePO_4$ electrode exhibited superior electrochemical performance in long-term cycling at high current rate. The cell also maintained

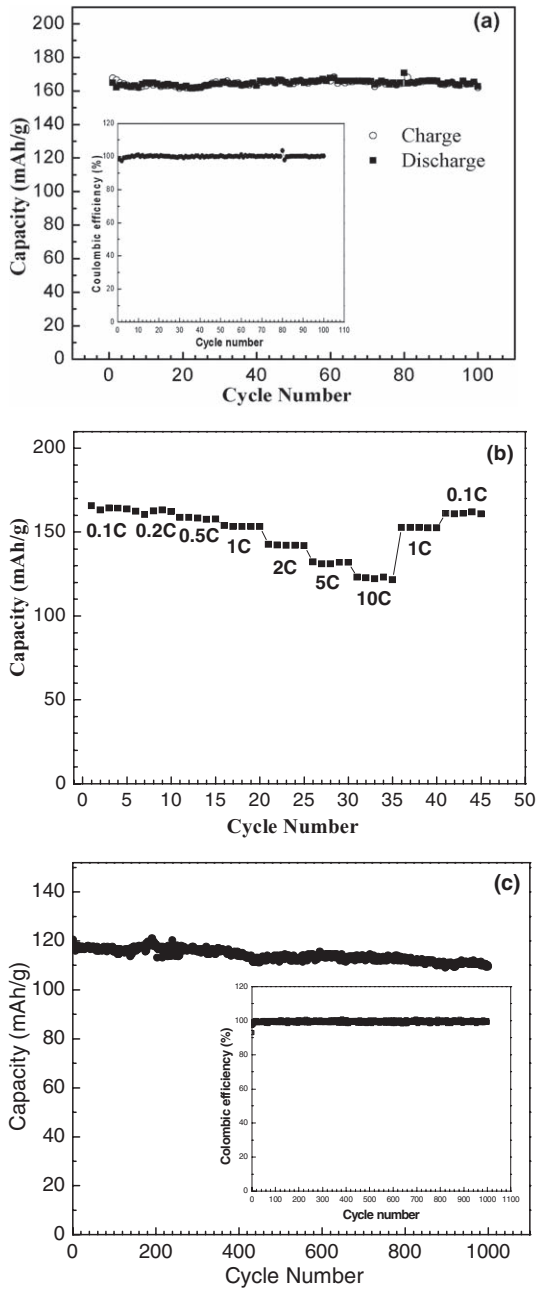

Figure 4. (a) Cycling performance mesoporous $LiFePO_4$/C nanocomposite electrode at the 0.1 C rate. The inset shows the coulombic efficiency (b) Rate performance of mesoporous $LiFePO_4$/C nanocomposite electrode at different current rates. (c) Discharge capacity *vs.* cycle number for mesoporous $LiFePO_4$/C nanocomposite electrode at the high rate of 10 C. The inset shows the high coulombic efficiency.

high coulombic efficiency, with an average value of 99.5% over 1000 cycles (as shown in the inset in Figure 4(c)). After 1000 cycles, the cell retained 91% of its initial capacity at the high 10 C rate. The average specific discharge capacity in 1000 cycles at the 10 C rate is about 115 mAh/g. Converting to specific power, the mesoporous $LiFePO_4$/C cathode delivered an average specific power of 4186 W/Kg and a specific energy of 283 Wh/g during 1000 cycles. To the best of our knowledge, this is the best high rate long-term cycling performance for $LiFePO_4$ cathode material reported so far. Such outstanding electrochemical performance certainly can meet the demands of many high power applications.

As shown in Figure 2(c) and (d), mesoporous $LiFePO_4$/C nanocomposite contains a mesoporous carbon framework, in which $LiFePO_4$ nanoparticles are homogeneously distributed both inside and outside mesopores. When assembled in lithium ion cells, liquid electrolyte can easily flood into the mesopores, ensuring high surface area contact with active $LiFePO_4$ nanocrystals. This effect induces fast lithium ion diffusion. Nanosize $LiFePO_4$ particles also provide a short path for lithium intercalation and de-intercalation. On the other hand, the carbon networks provide high electric conduction for electron transfer.[31–33] We further conducted ac impedance measurements on a freshly assembled test cell and again after three cycles (see the ac impedance spectra shown in SI Figure S7). A high charge-transfer resistance (R_{ct}) is a feature of the freshly assembled cell. However, the R_{ct} dramatically decreased after 3 charge/discharge cycles, indicating that the infiltration of the electrolyte into the mesopores plays an important role in reducing the polarisation. Therefore, the inflow of the electrolyte into the porous structure may affect the electrochemical performance in the initial cycles.[34] On the other hand, the decrease of R_{ct} could also be related to the destruction of passivation layer on the lithium metal surface.[35]

In conclusion, a highly ordered mesoporous $LiFePO_4$/C nanocomposite has been developed, in which $LiFePO_4$ nanoparticles are embedded in conductive and interconnected carbon networks. This mesoporous nanoarchitecture ensures not only intimate contact between liquid electrolyte and active $LiFePO_4$ nanoparticles, but also high electronic conductivity for both facile mass transfer and facile charge transfer. At the low current rate, mesoporous $LiFePO_4$/C nanocomposite cathodes delivered a near theoretical capacity with ultrahigh coulombic efficiency and capacity retention. At high current rate, the cell also exhibited a satisfactory specific capacity with an excellent cyclability. Through material architecture design, $LiFePO_4$ cathode material can meet the stringent requirements for high power applications such as electric vehicles and energy storage for smart grids.

Experimental Section

Materials synthesis: The synthesis of CMK-3 carbon templates were described in supporting information. For the synthesis of mesoporous $LiFePO_4$/C nanocomposite, CMK-3 template powders (0.1 g) were dispersed in concentrated HNO_3 (10 mL, >69%, Aldrich) and stirred for 1 hour at 80–90 °C to induce hydrophilicity. In the second step, lithium acetate (1 mmol, CH_3COOLi, 99%, Aldrich) and ferrous acetate (1 mmol, $(CH_3COO)_2Fe$, 99.95% trace metals basis, Aldrich) were dissolved into water (10 mL) and ethanol (10 mL) to form a transparent solution. Then, CMK-3 (0.1 g) was added into the solution, which was stirred overnight. The mixture was dried statically, grounded to powder, and then added into a solution containing ammonium dihydrogen phosphate (1 mmol, $NH_4H_2PO_4$, 98+%, Aldrich), H_2O (10 mL), and ethanol (10 mL). The mixture was stirred overnight, dried, ground, and sintered at 350 °C in Ar atmosphere to decompose the acetate. The same impregnation procedure was repeated once more to bring

about full utilization of the pores. The powder was finally sintered at 700 °C for 10 h in a H_2/Ar mixed gas to form the $LiFePO_4$ crystalline structure.

Materials characterisation: Small angle X-ray diffraction (SAXRD) patterns were collected on a Bruker D8 Advacned X-ray diffractometer using Cu Kα radiation. Wide angle X-ray diffraction (WAXRD) was conducted on a GBC MMA X-ray diffractometer with 2θ ranging from 20° to 70°. Raman spectra were recorded on a JOBIN Yvon Horiba Confocal Mico Raman spectrometer model HR 800 with 632.8 nm diode laser excitation on a 300 lines/mm grating at room temperature. N_2 adsorption–desorption isotherms were obtained using a Quadrasorb SI analyzer at 77 K. Brunauer-Emmett-Teller (BET) surface area was calculated using experimental points at a relative pressure of P/P_o = 0.05–0.25. The pore size distribution was calculated by the Barret-Joyner-Halenda (BJH) method. The porous structure and crystal structures of mesoporous $LiFePO_4$/C nanocomposites were characterized by TEM and HRTEM analysis (JEOL 2011 TEM facility).

Electrochemical testing: The electrodes were fabricated using a mixture of the prepared powders (80 wt%), carbon black (10 wt%), and polyvinylidene fluoride (PVDF 10 wt% Aldrich) in N-methyl-2-pyrrolidone (NMP) to form a slurry. The slurry was spread onto Al foil from a doctor blade and dried in an oven at 120 °C overnight under vacuum. The electrode area was 0.8 cm^2 and the loading of mesoporous $LiFePO_4$/C was 2 mg/cm^2. The electrochemical performance was tested by assembling CR2032 coin cells, using Li metal as the negative electrode. The electrolyte solution was 1 M $LiPF_6$ in a 1:1 mixture of ethylene carbonate (EC) and dimethyl carbonate (DMC). The galvanostatic charge and discharge experiment was performed in the range of 2.0–4.2 V at room temperature. Cyclic voltammetry (CV) and electrochemical impedance spectroscopy (EIS) measurements of the cells were carried out using a PARSTAT M2273 electrochemical workstation. For the EIS measurements, the amplitude of the AC signal to the cells was 5 mV and the frequency range was between 100 kHz and 10 mHz.

Supporting Information

Supporting Information is available from the Wiley Online Library or from the author.

Acknowledgements

This work was financially supported by the Australian Research Council (ARC) through Discovery project (DP0772999) and Linkage project (LP0989134) and the National Research Foundation of Korea through the WCU (World Class University) program (R32-2008-000-20093-0).

Received: June 3, 2010
Revised: July 13, 2010
Published online: September 14, 2010

[1] J. Tollefson, T. Scully, A. Witze, O. Morton, *Nature* **2008**, *454*, 818.
[2] D. Lindley, *Nature* **2010**, *463*, 18.
[3] J.-M. Tarascon, M. Armand, *Nature* **2001**, *414*, 359.
[4] M. Armand, J.-M. Tarascon, *Nature* **2008**, *451*, 652.
[5] A. K. Padhi, K. S. Nanjundaswamy, J. B. Goodenough, *J. Electrochem. Soc.* **1997**, *144*, 1188.
[6] A. K. Padhi, K. S. Nanjundaswamy, C. Masquelier, S. Okada, J. B. Goodenough, *J. Electrochem. Soc.* **1997**, *144*, 1609.
[7] F. Croce, A. D. Epifanio, J. Hassoun, A. Deptula, T. Olczac, B. Scrosati, *Electrochem. Solid State lett.* **2002**, *5*, A47.
[8] K. S. Park, J. T. Son, H. T. Chung, S. J. Kim, C. H. Lee, K. T. Kang, H. G. Kim, *Solid State Commun.* **2004**, *129*, A503.
[9] H. Huang, S. C. Yin, L. F. Nazar, *Electrochem. Solid State lett.* **2001**, *4*, 170.
[10] S. Y. Chung, J. T. Bloking, Y. M. Chiang, *Nature Mater.* **2002**, *1*, 123.
[11] G. X. Wang, S. Bewlay, J. Yao, J. H. Ahn, H. K. Liu, S. X. Dou, *Electrochem. Solid State lett.* **2004**, *7*, A503.
[12] S. Franger, F. L. Cras, C. Bourbon, H. Rouault, *Electrochem. Solid State lett.* **2002**, *5*, A231.
[13] Y. G. Wang, Y. R. Wang, E. Hosono, K. X. Wang, H. S. Zhou, *Angew. Chem. Int. Ed.* **2008**, *47*, 7461.
[14] P. Gibot, M. Casas-Cabanas, L. Laffont, S. Levasseur, P. Carlach, S. Hamelet, J.-M. Tarascon, C. Masquelier, *Nature Mater.* **2008**, *7*, 741.
[15] I. Bilecka, A. Hintennach, I. Djerdj, P. Novák, M. Niederger, *J. Mater. Chem.* **2009**, *19*, 5125.
[16] C. Delacourt, P. Poizot, S. Levassear, C. Masquelier, *Electrochem. Solid State lett.* **2009**, *9*, A352.
[17] Y. Q. Wang, J. L. Wang, J. Yang, Y. N. Nuli, *Adv. Func. Mater.* **2006**, *16*, 2135.
[18] H. M. Xie, R. S. Wang, J. R. Ying, L. Y. Zhang, A. F. Jalbout, H. Y. Yu, G. L. Yang, X. M. Pan, Z. M. Su, *Adv. Mater.* **2006**, *18*, 2135.
[19] S. Lim, C. S. Yoon, J. Cho, *Chem. Mater.* **2008**, *20*, 4560.
[20] B. Kang, G. Ceder, *Nature* **2009**, *458*, 190.
[21] a) S. Jun, S. H. Joo, R. Ryoo, M. Kruk, M. Jaroniec, Z. Liu, T. Ohsuna, O. Terasaki, *J. Am. Chem. Soc.* **2000**, *122*, 10712; b) R. Ryoo, S. H. Joo, M. Kruk, M. Jaroniec, *Adv. Mater.* **2001**, *13*, 677; c) C. Liang, Z. J. Li, S. Dai, *Angew. Chem. Int. Ed.* **2008**, *47*, 2.
[22] a) J. Chen, M. A. Hamon, H. Hu, Y. S. Chen, A. M. Rao, P. C. Eklund et al. *Science* **1998**, *282*, 95; b) J. Chen, A. M. Rao, S. Lyuksyutov, M. E. Itkis, M. A. Hamon, H. Hu, R. W. Cohn, P. C. Eklund, D. T. Colbert, R. E. Smalley, R. C. Haddon, *J. Phys. Chem. B* **2001**, *105*, 2525; c) S. Niyogi, M. A. Hamon, B. Zhao, P. Bhowmik, R. Sen, M. E. Itkis, R. C. Haddon, *Acc. Chem. Res.* **2002**, *35*, 1105.
[23] A. A. Salah, A. Mauger, C. M. Julien, F. Gendron, *Materials Science & Engineering B* **2006**, *129*, 232.
[24] P. S. Herle, B. Ellis, L. F. Nazar, *Nature Mater.* **2004**, *3*, 147.
[25] B. L. Ellis, W. R. M. Makahnouk, Y. Makimura, K. Toghill, L. F. Nazar, *Nature Mater.* **2007**, *6*, 749.
[26] a) R. Ryoo, C. H. Ko, M. Kruk, V. Antochshuk, M. Jaroniec, *J. Phys. Chem. B* **2000**, *104*, 11465; b) J. S. Lee, S. H. Joo, R. Ryoo, *J. Am. Chem. Soc.* **2002**, *124*, 1156.
[27] C. M. Doherty, R. A. Caruso, B. M. Smarsly, P. Adelhelm, C. J. Drummond, *Chem. Mater.* **2009**, *21*, 5300.
[28] X. L. Wu, L. Y. Jiang, F. F. Cao, Y. G. Guo, L. J. Wan, *Adv. Mater.* **2009**, *21*, 2710.
[29] a) E. M. Bauer, C. Bellitto, M. Pasquali, P. P. Prosini, *Electrochem. Solid State Lett.* **2004**, *7*, A85; b) P. P. Prosini, M. Carewska, S. Scaccia, P. Wisniewski, M. Pasquali, *Electrochim. Acta* **2003**, *48*, 4205; c) E. M. Bauer, C. Bellitto, G. Righini, M. Pasquali, A. Dell'Era, P. P. Prosini, *J. Power Sources* **2005**, *146*, 544.
[30] FreedomCar PHEV battery, http://www.uscar.org (last accessed 05-28-2010).
[31] X. L. Ji, K. T. Lee, L. F. Nazar, *Nature Mater.* **2009**, *8*, 500.
[32] I. Grigoriants, L. Sominski, H. L. Li, I. Ifargan, D. Aurbach, A. Gedanken, *Chem. Commun.* **2005**, 921.
[33] a) W. J. Cui, H. J. Liu, C. X. Wang, Y. Y. Xia, *Electrochem. Commun.* **2008**, *10*, 1587; b) P. G. Bruce, B. Scrosati, J.-M. Tarascon, *Angew. Chem. Int. Ed.* **2008**, *47*, 2930.
[34] a) K. M. Shaju, F. Jiao, A. Debart, P. G. Bruce, *Phys. Chem. Chem. Phys.* **2007**, *9*, 1837; b) X. W. Lou, D. Deng, J. Y. Lee, L. A. Archer, *J. Mater. Chem.* **2008**, *18*, 4397.
[35] D. Zane, M. Carewska, S. Scaccia, F. Cardellini, P. P. Prosini, *Electrochim. Acta* **2004**, *4*, 4259.